= 20.3 Hz) at this temperature. These couplings show that the γ-agostic interaction has σ-symmetry, with respect to the metal center. Otherwise no yttrium coupling on the interacting CH fragment would have been observed.

The spectroscopy of **16** clearly indicates the presence of a γ-agostic interaction in this complex between the Lewis acid yttrium and one of the ortho-CH bonds of the DMB ligand. This interaction is static at −80 °C, while at higher temperatures both ortho-CH bonds are involved due to dynamic processes like rotation and wagging.[3] Moreover, the NMR study of **16** demonstrates the potential of NMR spectroscopy when a metal center with a nuclear spin momentum, like yttrium, is present.

Conclusions

We have demonstrated that the σ-yttrium–carbon bond in 14- and 16-electron permethylyttrocene carbyls is extremely reactive toward virtually all hydrogen-containing bonds. Our studies on the activation of CH bonds clearly indicate that a rich organometallic chemistry is available on the basis of reactions with the YC bonds.

The reaction mechanisms of these activation reactions as well as the hydrogenolysis of the YC bond are likely to proceed via four or five centered transition states. These σ-bond metathesis reactions are a convenient way for the synthesis of new salt-free[4] permethylyttrocene derivatives. The Lewis acidity of the metal center is high as is clearly shown by the complexation of polar solvent molecules and the presence of a γ-agostic interaction in **16**. The nuclear spin momentum is of yttrium is very helpful in the unequivocal interpretation of complicated NMR spectra.

In addition to stoichiometric reactions also catalytic reactions have been found in which the YC bond plays a crucial role. Examples are the dimerizations of α-alkynes and H/D exchange reactions between sp^2-CD and sp^3-CH bonds.

The reactivity of the hydrides toward unsaturated hydrocarbons, carbonyls, and ethers also promises an interesting chemistry, and we are currently exploring this field. The results of these studies will be reported in a subsequent paper.

Registry No. **1**, 95197-83-4; **2**, 109364-77-4; **3**, 109364-78-5; **4**, 109364-79-6; **5**, 109364-80-9; **6**, 109364-81-0; **7a**, 109364-82-1; **7b**, 109364-92-3; **7c**, 109364-93-4; **8**, 109364-83-2; **9**, 109364-84-3; **10**, 926-55-6; **11**, 62676-19-1; **12**, 90753-17-6; **13**, 109364-85-4; **14**, 109364-86-5; **15**, 109364-87-6; **16**, 108366-50-3; **17**, 109364-88-7; **18a**, 95099-09-5; **18b**, 109364-89-8; **19a**, 109364-90-1; **19b**, 109364-91-2; $(Cp_2^*YCl)_2$, 94348-89-7; $Cp_2^*YCl\cdot THF$, 94348-90-0; $CH_2(SiMe_3)_2$, 2117-28-4; $HC{\equiv}CSiMe_3$, 1066-54-2; propyne, 74-99-7; phenylethyne, 536-74-3; pyridine, 110-86-1; α-picoline, 109-06-8; mesitylene, 108-67-8.

Syntheses and Molecular and Electronic Structures of the μ_4-Methylidyne Clusters $[Fe_4(CO)_{12}C\cdot C(O)OCH_3]^-$ and $[Fe_4(CO)_{12}C\cdot C(O)CH_3]^-$: An Analysis of Steric and Bonding Effects

John S. Bradley,* Suzanne Harris, John M. Newsam, Ernestine W. Hill, Susan Leta, and Michelle A. Modrick

Exxon Research and Engineering Company, Route 22 East, Clinton Township, Annandale, New Jersey 08801

Received December 5, 1986

The crystal, molecular, and electronic structures of $(C_2H_5)_4N[Fe_4(CO)_{12}C\cdot C(O)OCH_3]$, I, and $(C_2H_5)_4N[Fe_4(CO)_{12}C\cdot C(O)CH_3]$, II, which have served as the starting materials for a number of organometallic iron butterfly compounds, are described. Crystallographic data are as follows. I (296 K): space group *Pbca*, a = 12.079 (2) Å, b = 17.869 (4) Å, c = 27.692 (9) Å, Z = 8, R = 0.042, R_w = 0.055 for 2541 reflections ($I > 3\sigma(I)$), Mo Kα radiation. II (296 K): space group *Pbca*, a = 12.191 (7) Å, b = 17.296 (7) Å, c = 28.133 (7) Å, Z = 8; R = 0.037, R_w = 0.48 for 2932 reflections ($I > 2\sigma(I)$), Mo Kα radiation. Both cluster anions have an open butterfly core of four iron atoms with the methylidyne ligands $C\cdot CO_2CH_3$ (I) and $C\cdot C(O)CH_3$ (II) bound to all four metal atoms and the organic groups situated in the plane defined by the two backbone iron atoms and the methylidyne carbon atom. Comparisons are made between the molecular structures of I and II and those of the underivatized Fe_4C clusters. The differences between the two structure types are related to changes in the bonding between the μ_4-carbon and the iron framework. Interactive molecular graphics procedures were used to compute nonbonded atom–atom interaction energies as a probe of steric restrictions on the orientations of the carbomethoxy group in I and of the acetyl group in II. In both materials the organic groups are found to be sterically constrained to conformations close to those observed crystallographically. The observed slight tilt away from an axial orientation of the acetyl group in II is shown to mitigate steric repulsions between nonbonded atoms without disrupting strong orbital interactions between bonded atoms.

Introduction

The chemistry of the carbon atom in μ_4-carbido clusters has been of interest since the initial observations on the reactivity of the carbon atom in butterfly Fe_4C clusters.[1,2] This carbon atom forms bonds readily to carbon and to hydrogen, as in $[Fe_4(CO)_{12}C\cdot C(O)OCH_3]^-$[2] and $HFe_4(CO)_{12}CH$,[3] suggesting analogies with surface phenomena in metal-catalyzed CO hydrogenation. Several studies have been undertaken to determine the electronic structures of the Fe_4C family of cluster molecules and to correlate these with molecular structure and reactivity.[4-7] We have

(1) Bradley, J. S. *Adv. Organomet. Chem.* **1983**, *22*, 1–58.
(2) Bradley, J. S.; Ansell, G. B.; Hill, E. W. *J. Am. Chem. Soc.* **1979**, *101*, 7417–7419.
(3) Tachikawa, M.; Muetterties, E. L. *J. Am. Chem. Soc.* **1980**, *102*, 4541–4542.

0276-7333/87/2306-2060$01.50/0

synthesized and determined the structures of a number of Fe_4C derivatives, and we report here on the molecular and electronic structures of two clusters that have served as the precursors for a number of these materials, $[Fe_4(CO)_{12}C{\cdot}C(O)OCH_3]^-$, I, and $[Fe_4(CO)_{12}C{\cdot}C(O)CH_3]^-$, II. The latter was originally synthesized by Tachikawa and Muetterties,[8] but no crystal structure was reported. The essential features of the structure of the former were communicated earlier,[2] and we present here the full results of a more complete refinement of the structure. Comparisons are made between the molecular structures of I and II and the parent underivatized Fe_4C clusters, and we relate differences between the two structure types to changes in the bonding between the μ_4-carbon and the iron framework. Steric constraints on the orientations of the organic groups in I and II were explored by interactive molecular graphics.[9]

Experimental Section

1. Synthesis of the Clusters. All manipulations were carried out in either a nitrogen-filled drybox or on a double manifold vacuum line by using standard Schlenk glassware. Solvents were purified in the normal manner. The starting material for the cluster syntheses reported here is $(Et_4N)_2[Fe_6C(CO)_{16}]$, which was prepared from $Fe(CO)_5$ by the method of Churchill et al.[10] Satisfactory elemental analyses (Galbraith Laboratories, Knoxville, TN) were obtained for all materials. Infrared spectra were recorded on either a Beckman 4250 spectrophotometer or a Perkin Elmer IR 32 FT spectrophotometer.

Synthesis of $Et_4N[Fe_4(CO)_{12}C{\cdot}C(O)OCH_3]$, I. The synthesis of I, which is the tetranuclear starting material for all of our excursions in Fe_4C chemistry, has undergone various modifications during the course of our work in this area. The following procedure works well on quite a large scale and uses relatively inexpensive reagents ($FeCl_3$ and $Et_4N^+Br^-$).

$(Et_4N)_2[Fe_6C(CO)_{16}]$ (10 g, 9.5 mmol) was dissolved in methanol (1 L) containing an excess of tetraethylammonium bromide (10 g). Anhydrous iron(III) chloride (10.8 g, 7 equiv) was added in aliquots of ~1 g over a period of 15 min. The purple solution of the starting material became green-black, and after a further 15 min the reaction mixture was evaporated to dryness and washed with water. The black residue was dried in vacuo, washed with ether until the washings were colorless, and recrystallized from methylene chloride–hexane (50:50) by evaporation in a nitrogen stream. Yield: 5.2 g, 6.97 mmol, 70%. Infrared and ^{13}C and ^1H NMR revealed the product as indistinguishable from that prepared by our original method.[2] Anal. Calcd for $C_{23}H_{23}O_{14}Fe_4N$: C, 36.31; H, 3.04; N, 1.84. Found: C, 36.50; H, 3.04; N, 1.84.

Synthesis of $Et_4N[Fe_4(CO)_{12}C{\cdot}C(O)CH_3]$, II. II is prepared from $[Fe_4C(CO)_{12}]^{2-}$ and methyl iodide by a procedure essentially similar to that reported by Tachikawa and Muetterties.[8] Our synthesis of $[Fe_4C(CO)_{12}]^{2-}$ from $[Fe_4(CO)_{12}C{\cdot}C(O)OCH_3]^-$ via $[HFe_4C(CO)_{12}]^-$ proceeds in high yield from starting materials available in bulk; this is described here in full (see Scheme I).

i. $Et_4N[HFe_4C(CO)_{12}]$. $Et_4N[Fe_4(CO)_{12}C{\cdot}C(O)OCH_3]$ (1.0 g, 1.3 mmol), prepared as described above, in dry THF (100 mL) was treated with an excess of $BH_3{\cdot}THF$ (1.5 mL of a 1.0 M solution in THF) by slow addition via syringe. After 30 min of stirring, the green-black color of the starting material was converted to a deep red, and the infrared spectrum of the reaction mixture

Scheme I

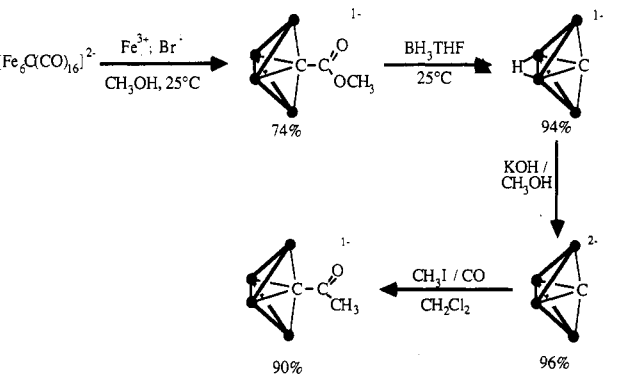

contained absorptions at 2015 (s), 2007 (s), 1987 (s), 1977 (m), 1965 (sh), and 1933 (m) cm^{-1}. Evaporation of the THF under reduced pressure followed by extraction into methylene chloride (100 mL) gave a deep red solution. Addition of hexane (~50 mL) and slow evaporation in a stream of nitrogen yielded the product as a black crystalline solid (0.90 g, 95%), with infrared and ^{13}C and ^1H NMR spectra consistent with those reported by Holt et al.[11] Anal. Calcd for $C_{21}H_{21}O_{12}Fe_4N$: C, 35.88; H, 3.01; N, 1.99. Found: C, 35.38; H, 3.00; N, 1.95.

ii. $(Et_4N)_2[Fe_4C(CO)_{12}]$. $Et_4N[HFe_4C(CO)_{12}]$ (1.0 g, 1.4 mmol) was dissolved in a solution of tetraethylammonium bromide (0.6 g, 2.9 mmol) in methanol (100 mL). Potassium hydroxide (0.16 g, 2.8 mmol) was added and the mixture stirred. After 15 min red-brown crystals of $(Et_4N)_2[Fe_4C(CO)_{12}]$ separated and were collected by filtration. After being washed with methanol and then diethyl ether, the product (1.1 g, 1.3 mmol, 94%) was dried in vacuo. If necessary this material may be recrystallized from acetone–2-propanol (60:40) by slow evaporation. IR (THF): 2037 (w), 1968 (s), 1945 (s), 1917 (w), 1892 (w) cm^{-1}. Anal. Calcd for $C_{29}H_{40}O_{12}Fe_4N_2$: C, 41.87; H, 4.85; N, 3.84. Found: C, 40.54; H, 4.85; N, 3.44.

iii. $Et_4N[Fe_4(CO)_{12}C{\cdot}C(O)CH_3]$, II. To a solution of $(Et_4N)_2[Fe_4C(CO)_{12}]$ (1.0 g, 1.2 mmol) in methylene chloride (200 mL) was added methyl iodide (0.4 g, 2.8 mmol), and the deep red mixture was refluxed for 24 h. The reaction mixture became intense green-black, with new infrared absorptions at 2060 (w), 2025 (s), 1992 (s), 1980 (sh), 1920 (w), and 1590 (w) cm^{-1}. (Sampling the solution for infrared analysis will generally result in loss of methyl iodide (bp 41 °C) and so in the event that the reaction is incomplete another 0.4 g is added and refluxing continued). Evaporation of the solvent gave a black residue, which was washed with cold water, dried in vacuo, and recrystallized from methylene chloride and hexane (50:50) by slow evaporation. (If the water wash and drying steps are not carried out, or are done with insufficient thoroughness, the yield is drastically reduced by the formation of trinuclear iron clusters, indicated by a red (instead of dark green) coloration of the methylene chloride extract.) Yield: 0.80 g, 1.1 mmol, 92%. (Given the stoichiometry of this reaction, this constitutes a quantitative yield, based on CO.) IR (THF): 2064 (vw), 2023 (s), 1985 (s), 1971 (sh), 1946 (w), 1598 (w) cm^{-1}. Anal. Calcd for $C_{23}H_{23}O_{13}Fe_4N$: C, 37.09, H, 3.11, N, 1.88. Found: C, 36.84; H, 3.42; N, 1.82.

2. X-ray Crystallography. X-ray Diffraction Study of $(Et_4N)[Fe_4(CO)_{12}C{\cdot}C(O)OCH_3]$, I. Black prismatic crystals of I were grown from methylene chloride–hexane solution by slow evaporation. Data were collected from a crystal approximately 0.20 × 0.20 × 0.20 mm mounted on a glass fiber on an Enraf-Nonius CAD4 automatic diffractometer. Table I contains crystal parameters and data collection details. Data collection lasted 147 h, and total intensity loss of only 0.6% was noted for three check reflections that had been monitored periodically during this time. Data were corrected for Lorentz and polarization factors. Of 5257 independent reflections, 2541 with $I > 3\sigma(I)$ were used in structure solution and refinement. The structure was solved by using direct methods (MULTAN, Enraf-Nonius, 1982) and difference Fourier syntheses. All non-hydrogen atoms were refined anisotropically.

(4) Kolis, J. W.; Basolo, F.; Shriver, D. F. *J. Am. Chem. Soc.* **1982**, *104*, 5626–5630.
(5) Housecroft, C. E.; Fehlner, T. P. *Organometallics* **1983**, *2*, 690. Fehlner, T. P.; Housecroft, C. E. *Organometallics* **1984**, *3*, 764.
(6) Wijeyesekera, S. D.; Hoffmann, R.; Wilder, C. N. *Organometallics* **1984**, *3*, 962–970.
(7) Harris, S.; Bradley, J. S. *Organometallics* **1984**, *3*, 1086–1093.
(8) Davis, J. H.; Beno, M. A.; Williams, J. M.; Zimmie, J.; Tachikawa, M.; Muetterties, E. L. *Proc. Natl. Acad. Sci. U.S.A.* **1981**, *78*, 668–671.
(9) Newsam, J. M.; Bradley, J. S. *J. Chem. Soc., Chem. Commun.* **1985**, 759–760.
(10) Churchill, M. R.; Wormald, J.; Knight, J.; Mays, M. J. *J. Am. Chem. Soc.* **1971**, *93*, 3073–3075.
(11) Holt, E. M.; Whitmire, K. H.; Shriver, D. F. *J. Organomet. Chem.* **1981**, *213*, 125–137.

Table I. X-ray Diffraction Data for $(Et_4N)[Fe_4(CO)_{12}C \cdot C(O)OCH_3]$, I, and $(Et_4N)[Fe_4(CO)_{12}C \cdot C(O)CH_3]$, II

A. Crystal Parameters		
formula	$C_{23}H_{23}O_{14}Fe_4N$, I	$C_{23}H_{23}O_{13}Fe_4N$, II
cryst system	orthorhombic	orthorhombic
space group	*Pbca*	*Pbca*
lattice constants (23 °C)		
a, Å	12.079 (2)	12.191 (7)
b, Å	17.869 (4)	17.296 (7)
c, Å	27.692 (9)	28.133 (7)
V, Å^3	5977	5932
z	8	8
mol wt	760.8	744.8
γ(calcd) g cm^{-3}	1.691	1.668
B. Data Collection		
radiation	Mo K$\bar{\alpha}$(λ = 0.710 730 Å)	
monochromator	graphite	
scan range, deg	$0 < 2\theta \leftarrow < 50$	$0 < 2\theta < 50$
scan type	ω–2θ	ω–2θ
scan rate, deg/min	2–13	2–20
reflectns examined	5854	5967
independent reflectns	5257	5796
reflectns obsd	2541 ($I > 3\sigma(I)$)	2932 ($I > 2\sigma(I)$)
cryst stability: std reflectns	no decay	2.8% decay over data collectn period; linear correctn applied

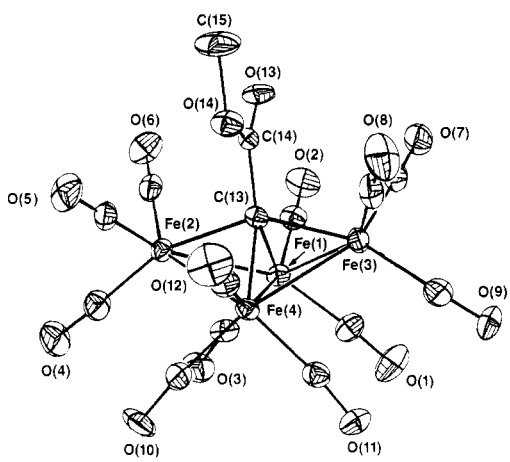

Figure 1. ORTEP drawing of $[Fe_4(CO)_{12}C \cdot C(O)OCH_3]^-$, I, showing 30% probability thermal ellipsoids. Only oxygen atoms for the carbonyls are numbered and these define the carbon atom numbering scheme.

Some of the hydrogen atoms on the tetraethylammonium cation were located by difference Fourier synthesis. The remainder were assigned idealized positions. Full-matrix least-squares refinement converged to residuals of $R = 0.037$ and $R_w = 0.048$ ($R = \sum||F_o| - |F_c||/\sum|F_o|$ and $R_w = (\sum w(|F_o| - |F_c|)^2/\sum|F_o|^2)^{1/2}$). Atomic coordinates are listed in Table II and bond lengths and angles in Tables IV and V. Figure 1 is a view of the molecular structure of the anion, indicating the atom numbering scheme.

X-ray Diffraction Study of $(Et_4N)[Fe_4(CO)_{12}C \cdot C(O)CH_3]$, II. Black prismatic crystals of II were grown from methylene chloride–hexane solution, and data were collected at Molecular Structures Corp., College Station, TX, on a crystal with approximate dimensions 0.30 × 0.25 × 0.15 mm mounted on a glass fiber. Table I contains details of the crystal parameters and data collection. Data were corrected for absorption, Lorentz, and polarization factors. Of the 5796 independent reflections, 2932 were considered observed ($I > 2\sigma(I)$) and used in refinement of the structure. Periodically monitored check reflections revealed a loss of intensity of ca. 3% over the course of data collection, and a linear decay correction was applied.

Direct methods (MULTAN, Enraf-Nonius, 1982) were used to determine the locations of the four iron atoms, and the positions of the other non-hydrogen atoms were determined by a series of difference Fourier syntheses. Full-matrix least-squares refinement converged to residuals of $R = 0.042$ and $R_w = 0.055$. Forty-one non-hydrogen atoms were refined with anisotropic thermal parameters. The hydrogen atoms were located by difference Fourier synthesis, and refined with isotropic thermal parameters. Atomic coordinates are listed in Table III and bond lengths and angles in Tables IV and V. Figure 2 indicates the atom numbering scheme for the anion.

Table II. Positional Parameters and Their Estimated Standard Deviations for $Et_4N[Fe_4(CO)_{12}C \cdot C(O)OCH_3]$, I[a]

atom	*x*	*y*	*z*	*B*, Å^2
Fe(1)	0.58976 (8)	0.46279 (5)	0.87687 (3)	2.66 (2)
Fe(2)	0.71813 (8)	0.54131 (5)	0.92584 (3)	2.74 (2)
Fe(3)	0.59376 (8)	0.52740 (5)	0.79707 (3)	2.93 (2)
Fe(4)	0.77408 (7)	0.51142 (5)	0.84107 (3)	2.50 (2)
O(1)	0.5426 (6)	0.3404 (3)	0.8103 (2)	7.1 (2)
O(2)	0.3657 (4)	0.4849 (3)	0.9142 (2)	5.5 (1)
O(3)	0.6643 (5)	0.3542 (3)	0.9476 (2)	5.5 (1)
O(4)	0.8432 (5)	0.4640 (3)	1.0005 (2)	6.6 (2)
O(5)	0.8615 (5)	0.6717 (3)	0.9334 (2)	5.7 (1)
O(6)	0.5370 (4)	0.5870 (3)	0.9893 (2)	5.4 (1)
O(7)	0.3569 (4)	0.5569 (3)	0.8037 (2)	5.0 (1)
O(8)	0.6546 (5)	0.6617 (3)	0.7421 (2)	6.6 (2)
O(9)	0.5799 (5)	0.4386 (4)	0.7086 (2)	7.2 (2)
O(10)	0.9464 (4)	0.4340 (3)	0.8951 (2)	6.4 (1)
O(11)	0.8086 (4)	0.4075 (3)	0.7615 (2)	4.9 (1)
O(12)	0.9129 (4)	0.6348 (3)	0.8058 (2)	5.9 (1)
O(13)	0.5103 (4)	0.6600 (2)	0.8820 (2)	3.8 (1)
O(14)	0.6772 (4)	0.6921 (2)	0.8526 (2)	3.7 (1)
N(1)	0.7789 (4)	0.2401 (3)	0.5919 (2)	2.9 (1)
C(1)	0.5622 (6)	0.3917 (4)	0.8337 (3)	4.1 (2)
C(2)	0.4539 (6)	0.4760 (4)	0.8996 (3)	3.7 (2)
C(3)	0.6394 (6)	0.4004 (4)	0.9216 (3)	3.9 (2)
C(4)	0.7935 (7)	0.4930 (4)	0.9712 (3)	4.3 (2)
C(5)	0.8060 (6)	0.6210 (4)	0.9298 (3)	3.4 (2)
C(6)	0.6084 (6)	0.5683 (4)	0.9653 (3)	3.5 (2)
C(7)	0.4490 (6)	0.5456 (4)	0.8004 (2)	3.5 (2)
C(8)	0.6333 (6)	0.6101 (4)	0.7635 (3)	4.2 (2)
C(9)	0.5849 (6)	0.4712 (4)	0.7432 (3)	4.6 (2)
C(10)	0.8769 (6)	0.4659 (4)	0.8764 (3)	3.8 (2)
C(11)	0.7887 (6)	0.4493 (4)	0.7912 (3)	3.4 (2)
C(12)	0.8596 (6)	0.5863 (4)	0.8196 (3)	3.5 (2)
C(13)	0.6421 (5)	0.5641 (3)	0.8624 (2)	2.4 (1)
C(14)	0.6008 (5)	0.6421 (3)	0.8673 (2)	2.6 (1)
C(15)	0.6439 (8)	0.7708 (4)	0.8555 (4)	6.4 (2)
C(16)	0.6768 (5)	0.2703 (4)	0.5664 (3)	3.5 (2)
C(17)	0.6729 (6)	0.3548 (4)	0.5620 (3)	4.5 (2)
C(18)	0.7638 (6)	0.1563 (3)	0.5938 (3)	3.4 (2)
C(19)	0.8573 (7)	0.1137 (4)	0.6148 (3)	4.4 (2)
C(20)	0.8843 (6)	0.2607 (4)	0.5660 (3)	3.9 (2)
C(21)	0.8926 (6)	0.2340 (5)	0.5146 (3)	5.3 (2)
C(22)	0.7891 (6)	0.2727 (4)	0.6423 (3)	4.1 (2)
C(23)	0.6898 (6)	0.2636 (5)	0.6748 (3)	4.9 (2)
H(1)	0.672	0.247	0.533	
H(2)	0.609	0.253	0.585	
H(3)	0.604	0.372	0.545	
H(4)	0.677	0.379	0.594	
H(5)	0.739	0.372	0.542	
H(6)	0.695	0.144	0.613	
H(7)	0.751	0.137	0.559	
H(8)	0.844	0.058	0.615	
H(9)	0.929	0.122	0.596	
H(10)	0.872	0.130	0.649	
H(11)	0.896	0.317	0.567	
H(12)	0.951	0.238	0.584	
H(13)	0.965	0.250	0.499	
H(14)	0.885	0.179	0.512	
H(15)	0.830	0.258	0.495	
H(16)	0.854	0.249	0.660	
H(17)	0.805	0.328	0.640	
H(18)	0.701	0.287	0.708	
H(19)	0.622	0.289	0.660	
H(20)	0.671	0.209	0.680	

[a] Hydrogen atom temperature factors were fixed at $B = 5.0$ Å^2. Anisotropically refined atoms are given in the form of the isotropic equivalent thermal parameter defined as: $(4/3)[a^2B(1,1) + b^2B(2,2) + c^2B(3,3) + ab(\cos\gamma)B(1,2) + ac(\cos\beta)B(1,3) + bc(\cos\alpha)B(2,3)]$.

Table III. Positional Parameters and Their Estimated Standard Deviations for $Et_4N[Fe_4(CO)_{12}C \cdot C(O)CH_3]$, II[a]

atom	x	y	z	B, Å²
Fe(1)	0.09538 (7)	0.04094 (5)	0.62423 (3)	3.17 (2)
Fe(2)	0.22346 (7)	−0.04138 (5)	0.57630 (3)	3.12 (2)
Fe(3)	0.09887 (7)	−0.02951 (5)	0.70258 (3)	3.54 (2)
Fe(4)	0.27657 (7)	−0.00864 (5)	0.65979 (3)	3.14 (2)
O(1)	0.0490 (6)	0.1697 (3)	0.6884 (2)	8.9 (2)
O(2)	−0.1273 (4)	0.0162 (3)	0.5883 (2)	6.0 (1)
O(3)	0.1627 (5)	0.1517 (3)	0.5515 (2)	6.7 (1)
O(4)	0.3505 (5)	0.0400 (3)	0.5040 (2)	7.7 (2)
O(5)	0.3729 (4)	−0.1716 (3)	0.5677 (2)	6.0 (1)
O(6)	0.0475 (4)	−0.0837 (3)	0.5110 (2)	5.8 (1)
O(7)	−0.1365 (4)	−0.0593 (3)	0.6968 (2)	6.0 (1)
O(8)	0.1639 (5)	−0.1627 (3)	0.7593 (2)	7.3 (2)
O(9)	0.0769 (5)	0.0636 (4)	0.7888 (2)	9.4 (2)
O(10)	0.4332 (5)	0.0873 (4)	0.6082 (2)	9.2 (2)
O(11)	0.3056 (4)	0.0984 (3)	0.7395 (2)	7.1 (1)
O(12)	0.4285 (4)	−0.1271 (3)	0.6935 (2)	6.7 (1)
O(13)	0.0071 (3)	−0.1521 (2)	0.6138 (2)	4.4 (1)
N(1)	0.2707 (4)	0.2425 (3)	0.4094 (2)	3.1 (1)
C(1)	0.0667 (6)	0.1161 (4)	0.6653 (3)	5.6 (2)
C(2)	−0.0401 (6)	0.0251 (3)	0.6023 (2)	3.9 (1)
C(3)	0.1399 (6)	0.1051 (4)	0.5794 (3)	4.4 (2)
C(4)	0.2997 (6)	0.0108 (4)	0.5323 (2)	4.7 (2)
C(5)	0.3133 (5)	−0.1213 (4)	0.5718 (2)	3.8 (1)
C(6)	0.1160 (5)	−0.0668 (3)	0.5359 (2)	3.7 (1)
C(7)	−0.0454 (6)	−0.0481 (4)	0.6994 (2)	4.3 (2)
C(8)	0.1391 (6)	−0.1107 (4)	0.7373 (2)	5.0 (2)
C(9)	0.0850 (6)	0.0284 (4)	0.7551 (3)	5.6 (2)
C(10)	0.3693 (6)	0.0476 (4)	0.6262 (3)	5.3 (2)
C(11)	0.2869 (5)	0.0551 (4)	0.7098 (3)	4.6 (2)
C(12)	0.3690 (5)	−0.0807 (4)	0.6797 (2)	4.1 (1)
C(13)	0.1463 (5)	−0.0649 (3)	0.6377 (2)	2.6 (1)
C(14)	0.0987 (5)	−0.1436 (3)	0.6307 (2)	3.3 (1)
C(15)	0.1639 (6)	−0.2133 (4)	0.6455 (3)	4.5 (2)
C(16)	0.2570 (5)	0.1556 (4)	0.4078 (2)	3.9 (1)
C(17)	0.3487 (7)	0.1110 (4)	0.3859 (3)	5.2 (2)
C(18)	0.3761 (5)	0.2655 (4)	0.4345 (3)	4.1 (2)
C(19)	0.3876 (6)	0.2366 (4)	0.4848 (3)	5.7 (2)
C(20)	0.1704 (5)	0.2740 (4)	0.4353 (2)	3.7 (1)
C(21)	0.1655 (6)	0.3604 (4)	0.4399 (3)	5.8 (2)
C(22)	0.2778 (6)	0.2766 (4)	0.3595 (2)	4.3 (2)
C(23)	0.1772 (6)	0.2657 (4)	0.3292 (3)	5.0 (2)
H(1)	0.163 (4)	−0.247 (3)	0.624 (2)	3 (1)*
H(2)	0.240 (4)	−0.203 (2)	0.659 (2)	2 (1)*
H(3)	0.116 (5)	−0.249 (3)	0.665 (2)	5 (2)*
H(4)	0.246 (4)	0.140 (3)	0.441 (2)	3 (1)*
H(5)	0.188 (5)	0.145 (3)	0.388 (2)	5 (2)*
H(6)	0.417 (5)	0.117 (3)	0.403 (2)	6 (2)*
H(7)	0.308 (7)	0.050 (4)	0.386 (3)	10 (2)*
H(8)	0.361 (4)	0.125 (3)	0.356 (2)	4 (1)*
H(9)	0.434 (4)	0.248 (3)	0.415 (2)	2 (1)*
H(10)	0.378 (3)	0.315 (2)	0.433 (1)	1 (1)*
H(11)	0.386 (5)	0.184 (4)	0.484 (2)	7 (2)*
H(12)	0.334 (6)	0.260 (4)	0.503 (3)	8 (2)*
H(13)	0.444 (4)	0.257 (3)	0.500 (2)	4 (1)*
H(14)	0.176 (3)	0.248 (2)	0.461 (2)	2 (1)*
H(15)	0.101 (4)	0.249 (3)	0.416 (2)	3 (1)*
H(16)	0.102 (5)	0.376 (3)	0.455 (2)	6 (2)*
H(17)	0.165 (5)	0.387 (3)	0.409 (2)	4 (1)*
H(18)	0.226 (4)	0.381 (3)	0.458 (2)	3 (1)*
H(19)	0.284 (5)	0.323 (3)	0.365 (2)	5 (1)*
H(20)	0.331 (4)	0.255 (3)	0.348 (2)	3 (1)*
H(21)	0.111 (5)	0.299 (3)	0.340 (2)	6 (2)*
H(22)	0.191 (5)	0.300 (3)	0.302 (2)	5 (2)*
H(23)	0.153 (5)	0.210 (3)	0.324 (2)	5 (2)*

[a] Atoms with an asterisk were refined isotropically. Anisotropically refined atoms are given in the form of the isotropic equivalent thermal parameters defined as: $(4/3)[a^2B(1,1) + b^2B(2,2) + c^2B(3,3) + ab(\cos\gamma)B(1,2) + ac(\cos\beta)B(1,3) + bc(\cos\alpha)B(2,3)]$.

Molecular Orbital Calculations. Molecular orbital (MO) calculations, using the Fenske–Hall method,[12] were carried out for both $[Fe_4(CO)_{12}C \cdot C(O)OCH_3]^-$, I, and $[Fe_4(CO)_{12}C \cdot C(O)CH_3]^-$, II. The iron 1s through 3d basis functions were taken from Richardson et al.[13] while the 4s and 4p functions were chosen to have exponents of 2.0. The carbon and oxygen functions were taken from the double-ζ 2p functions of Clementi.[14] The double-ζ 2p valence functions were retained while the 1s and 2s functions

(12) Hall, M. B.; Fenske, R. F. *Inorg. Chem.* **1972**, *11*, 768.

Table IV. Bond Distances (Å) in $Et_4N[Fe_4(CO)_{12}C \cdot C(O)OCH_3]$, I, and $Et_4N[Fe_4(CO)_{12}C \cdot C(O)CH_3]$, II, with Estimated Standard Deviations

	I	II
	Iron–Iron	
Fe(1)–Fe(2)	2.492 (1)	2.507 (1)
Fe(1)–Fe(3)	2.494 (1)	2.519 (1)
Fe(1)–Fe(4)	2.587 (1)	2.572 (1)
Fe(2)–Fe(4)	2.501 (1)	2.501 (1)
Fe(3)–Fe(4)	2.512 (1)	2.504 (1)
	Iron–Carbon (carbide)	
Fe(1)–C(13)	1.959 (6)	1.970 (6)
Fe(2)–C(13)	2.024 (6)	2.008 (6)
Fe(3)–C(13)	2.010 (6)	2.011 (6)
Fe(4)–C(13)	1.942 (6)	1.964 (6)
	Iron–Carbon (carbonyl)	
Fe(1)–C(1)	1.776 (7)	1.773 (8)
Fe(1)–C(2)	1.773 (8)	1.784 (8)
Fe(1)–C(3)	1.770 (8)	1.765 (8)
Fe(2)–C(4)	1.775 (8)	1.791 (8)
Fe(2)–C(5)	1.780 (7)	1.768 (8)
Fe(2)–C(6)	1.785 (8)	1.790 (8)
Fe(3)–C(7)	1.781 (8)	1.791 (9)
Fe(3)–C(8)	1.810 (8)	1.780 (9)
Fe(3)–C(9)	1.802 (9)	1.792 (9)
Fe(4)–C(10)	1.778 (8)	1.766 (8)
Fe(4)–C(11)	1.780 (8)	1.792 (8)
Fe(4)–C(12)	1.792 (8)	1.772 (8)
	Carbon–Oxygen	
C(1)–O(1)	1.147 (8)	1.155 (9)
C(2)–O(2)	1.151 (8)	1.145 (8)
C(3)–O(3)	1.136 (8)	1.160 (9)
C(4)–O(4)	1.135 (8)	1.130 (8)
C(5)–O(5)	1.132 (8)	1.140 (8)
C(6)–O(6)	1.139 (8)	1.128 (8)
C(7)–O(7)	1.135 (8)	1.129 (9)
C(8)–O(8)	1.125 (8)	1.133 (9)
C(9)–O(9)	1.123 (9)	1.131 (9)
C(10)–O(10)	1.139 (8)	1.155 (9)
C(11)–O(11)	1.137 (8)	1.144 (8)
C(12)–O(12)	1.146 (8)	1.149 (8)
	Methylidyne Group	
C(13)–C(14)	1.488 (8)	1.492 (9)
C(14)–O(13)	1.209 (7)	1.222 (7)
C(15)–C(14)		1.503 (10)
C(14)–O(14)	1.347 (7)	
C(15)–O(14)	1.465 (8)	

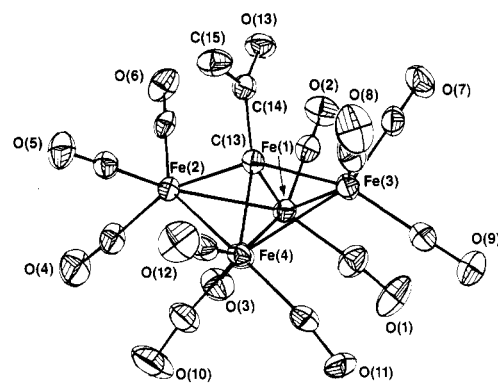

Figure 2. ORTEP drawing of $[Fe_4(CO)_{12}C \cdot C(O)CH_3]^-$, II, showing 30% probability thermal ellipsoids.

(13) Richardson, J. W.; Nieupoort, W. C.; Powell, R. R.; Egell, W. F. *J. Chem. Phys.* **1962**, *36*, 1057.
(14) Clementi, E. *J. Chem. Phys.* **1964**, *408* 1944; *IBM J. Res. Dev.* **1965**, *9*, 2.

Table V. Bond Angles (deg) in $Et_4N[Fe_4(CO)_{12}C \cdot C(O)OCH_3]$, I, and $Et_4N[Fe_4(CO)_{12}C \cdot C(O)CH_3]$, II, with their Estimated Standard Deviations

	I	II
Iron–Iron–Iron		
Fe(2)–Fe(1)–Fe(3)	102.10 (4)	100.68 (4)
Fe(2)–Fe(1)–Fe(4)	58.94 (3)	59.00 (3)
Fe(3)–Fe(1)–Fe(4)	59.22 (4)	58.93 (4)
Fe(1)–Fe(2)–Fe(4)	62.42 (4)	61.80 (4)
Fe(1)–Fe(3)–Fe(4)	62.25 (4)	61.60 (4)
Fe(1)–Fe(4)–Fe(2)	58.63 (4)	59.48 (4)
Fe(1)–Fe(4)–Fe(3)	58.53 (4)	59.20 (4)
Fe(2)–Fe(4)–Fe(3)	101.35 (4)	101.23 (4)
Iron–Carbon (carbide)–Iron		
Fe(1)–C(13)–Fe(2)	77.4 (2)	78.1 (2)
Fe(1)–C(13)–Fe(3)	77.8 (2)	78.5 (2)
Fe(1)–C(13)–Fe(4)	83.1 (2)	81.6 (2)
Fe(2)–C(13)–Fe(3)	147.9 (3)	148.6 (2)
Fe(2)–C(13)–Fe(4)	78.1 (2)	78.1 (2)
Fe(3)–C(13)–Fe(4)	78.9 (2)	78.1 (2)
Iron–Carbon (carbonyl)–Oxygen		
Fe(1)–C(1)–O(1)	172.0 (7)	173.5 (8)
Fe(1)–C(2)–O(2)	179.6 (6)	179.0 (6)
Fe(1)–C(3)–O(3)	172.1 (7)	174.1 (7)
Fe(2)–C(4)–O(4)	178.0 (7)	176.2 (7)
Fe(2)–C(5)–O(5)	178.5 (7)	177.7 (7)
Fe(2)–C(6)–O(6)	177.7 (7)	178.7 (7)
Fe(3)–C(7)–O(7)	178.3 (7)	179.0 (7)
Fe(3)–C(8)–O(8)	177.9 (8)	179.4 (9)
Fe(3)–C(9)–O(9)	177.4 (8)	178.4 (9)
Fe(4)–C(10)–O(10)	173.6 (7)	173.5 (8)
Fe(4)–C(11)–O(11)	172.6 (7)	171.6 (7)
Fe(4)–C(12)–O(12)	179.0 (7)	178.7 (7)
Carbon–Iron–Carbon		
C(1)–Fe(1)–C(2)	99.3 (3)	98.9 (4)
C(1)–Fe(1)–C(3)	94.8 (3)	93.8 (4)
C(2)–Fe(1)–C(3)	98.6 (3)	97.7 (3)
C(4)–Fe(2)–C(5)	92.3 (3)	91.3 (3)
C(4)–Fe(2)–C(6)	94.5 (4)	93.7 (4)
C(5)–Fe(2)–C(6)	100.9 (3)	102.5 (3)
C(7)–Fe(3)–C(8)	97.8 (3)	99.0 (4)
C(7)–Fe(3)–C(9)	94.9 (3)	92.8 (3)
C(8)–Fe(3)–C(9)	92.6 (4)	90.8 (4)
C(10)–Fe(4)–C(11)	94.1 (3)	92.1 (4)
C(10)–Fe(4)–C(12)	97.0 (3)	98.6 (4)
C(11)–Fe(4)–C(12)	98.6 (3)	98.0 (3)
Iron–Carbon (carbide)–Methylidyne		
Fe(1)–C(13)–C(14)	137.6 (5)	134.4 (5)
Fe(2)–C(13)–C(14)	105.1 (4)	104.7 (4)
Fe(3)–C(13)–C(14)	106.9 (4)	106.6 (4)
Fe(4)–C(13)–C(14)	139.2 (5)	143.9 (5)
Methylidyne Angles		
O(13)–C(14)–O(14)	123.1 (6)	
C(14)–O(14)–C(15)	115.6 (5)	
C(13)–C(14)–O(13)	125.6 (6)	121.1 (6)
C(13)–C(14)–O(14)	111.3 (6)	
C(13)–C(14)–C(15)		119.2 (6)
C(15)–C(14)–O(13)		119.6 (6)
Selected Torsional Angles		
Fe(3)–Fe(4)–C(1)	66.8	69.6
Fe(3)–Fe(4)–Fe(1)–C(2)	−62.4	−59.3
Fe(3)–Fe(4)–Fe(1)–C(3)	163.3	165.6
Fe(3)–Fe(1)–Fe(4)–C(10)	−165.2	−162.3
Fe(3)–Fe(1)–Fe(4)–C(11)	−68.4	−68.7
Fe(3)–Fe(1)–Fe(4)–C(12)	60.8	63.9

were reduced to single-ζ form. An exponent of 1.2 was used for hydrogen. Mulliken population analyses were used to determine atomic charges and orbital populations. Atomic positions used in the calculations were taken from the crystal structures of I and II (using hydrogen atom positions determined geometrically—see below) and were not idealized to C_s symmetry. For this reason the overlap populations listed in Table VI for $[Fe_4(CO)_{12}C \cdot C(O)OCH_3]^-$ vary slightly from those reported earlier on the basis of calculations for an idealized structure.[7]

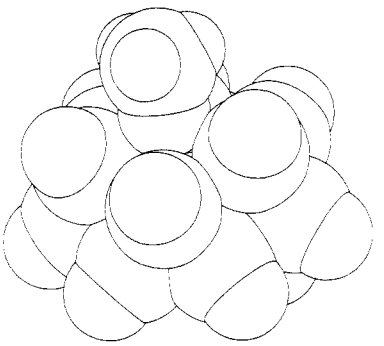

Figure 3. The molecular structure of the carbomethoxy derivative I drawn in approximately the same orientation as in Figure 1 with full van der Waals radii (drawing radii: C, 1.77, O, 1.40, H, 1.17; Fe, arbitrarily, 1.48 Å). The iron atoms are almost completely obscured and the importance of the carbonyl groups in dictating the steric environment of the ester function is apparent.

Interactive Molecular Graphics. In considering the steric environments of organic groups in the iron butterfly clusters, interactive molecular graphics routines were used to modify the molecular structures determined crystallographically (see below), to visualise the relative sizes of the cluster components and the interactions between them, and to compute relative nonbonded interaction energy sums for differing cluster conformations.

All the molecular modeling calculations were performed by using the CHEMGRAF program package[28] as implemented without modification on a VAX 11/750 computer system. The interactive molecular graphics manipulations were performed by using a Lundy R5688 graphics terminal and associated Summagraphics Bit Pad One digitising tablet connected to the VAX 11/750 via an in-house IBX phone system, using a 9600 baud line. The plots shown in the figures were produced on an IBM XY/750 8-pen plotter from a CHEMGRAF metafile of graphics primitive instructions. Color pictures (not included in the present report for economic reasons) were taken with a VideoSlide 35 camera unit that accepts the red-green-blue video signals from the monitor or by using a Nikon FM2 with a 80-mm Nikkor lens mounted directly on a tripod in front of the monitor.

The nonbonded interactions were modeled by using the expression and parameters given by a Del Re et al.[15] In applying these parameters (derived for organic systems) to organometallic components, we are making the assumption that the nonbonded interactions involving the carbon and oxygen atoms in a carbonyl group, for example, can be described in the same manner as those for the corresponding atoms in an organic molecule such as acetone. This is an approximation, because even in organic molecules the effective van der Waals radius of a given atom depends on its coordination environment.[16] Although suitable nonbonded interaction energy parameters for the iron atoms are unavailable, the steric restraints in clusters of this type are dominated by the ligand–ligand interactions (Figure 3). Omitting contributions from the metal atoms therefore does not significantly affect the calculations of relative steric energies.

Perhaps the most important limitation in this approach is an inability to accomodate overall molecular relaxations. The equilibrium configuration of an organometallic molecule represents a minimum in the total energy sum, to which the nonbonded components form only one contribution. The nonbonding energy debit associated with a sterically unfavorable configuration may thus be lessened to a certain degree by slight readjustments of the cluster bond lengths, angles, and torsion angles. Established molecular mechanics procedures that consider such effects have been extremely successful in modeling the configurations of organic systems in which structural, thermodynamic, and spectroscopic data for a range of similar compounds are available[17–20]

(15) Del Re, G.; Gavuzzo, E.; Giglio, E.; Lelj, F.; Mazza, F.; Zappia, V. *Acta Crystallogr., Sect. B: Struct. Crystallogr. Cryst. Chem.* **1977**, *B33*, 3289–3296.

(16) Francl, M. M.; Hour, R. F.; Hehre, W. J. *J. Am. Chem. Soc.* **1984**, *106*, 563–570.

(17) Allinger, N. L. *J. Am. Chem. Soc.* **1977**, *99*, 8127–8134.

Table VI. Overlap Populations

	$[Fe_4C(CO)_{12}]^{2-}$[a]		$[Fe_4(CO)_{12}C\cdot C(O)OCH_3]^-$		$[Fe_4(CO)_{12}C\cdot C(O)CH_3]^-$		
	Fe_w[b]	Fe_b[c]	Fe_w	Fe_b	Fe_w	Fe_1	Fe_4
$C(p_x)$–Fe(d,s,p)	0.040	0.084	0.010	0.112	0.013	0.126	0.097
$C(p_y)$–Fe(d,s,p)	0.162	0.000	0.124	0.004	0.124	0.003	0.004
$C(p_z)$–Fe(d,s,p)	0.047	0.081	0.005	0.059	0.005	0.049	0.070
total C p–Fe(d,s,p)	0.249	0.165	0.139	0.175	0.142	0.178	0.171

[a] Reference 7. [b] Wingtip iron. [c] Backbone iron.

and where the bonding of a particular species in a variety of environments is inherently similar. For most organometallic systems neither of these conditions pertain, and although considerable progress is being made,[21-27] general force fields are not yet available for systems of the present type.

The present modeling methods therefore consider only nonbonded terms as the configurations of one or more groups are adjusted with respect to the remainder of the assumed rigid or near-rigid molecular framework. The success of these assumptions is gauged by considering the modeling results in comparison with X-ray crystallographic data, synthesis results, and the outcome of detailed MO analyses of selected conformations. The individual Mulliken atomic charges, which the MO analyses provide, were also used in computing coulombic contributions to the nonbonded energy sum.

The coordinates of all non-hydrogen atoms of the carbomethoxy derivative $[Fe_4(CO)_{12}C\cdot C(O)OCH_3]^-$, I, were taken from the single-crystal X-ray analysis of the tetraethylammonium salt (Table II). The three protons H(34), H(35), and H(36) of the methyl group were added geometrically to satisfy C–H bond distances of 1.000 Å, O(14)–C(15)–H angles of 110.0°, and H–C(15)–H angles of 108.9°. Dummy atoms V1 and V2 were added at points on the vectors defined as the cross-products of the $\overline{C(13)-C(14)}$ vector and the $\overline{C(13)-Fe(2)}$ and the $\overline{C(13)-Fe(1)}$ vectors, respectively. These dummy atoms provide fulcra such that changes in the Fe(1)–C(13)–C(14) angle (ϕ) and the Fe(2)–C(13)–C(14) angle (χ) could be effected by rotations about the C(13)–V2 and C(13)–V1 connections, respectively. Such rotations track the carbomethoxy group only approximately in the C(13)Fe(1)Fe(4) and C(13)Fe(2)Fe(3) planes, respectively, because C(14) lies exactly in neither of these planes. The nonbonded interaction energy summations over all nonbonded atom pairs were then computed as a function three molecular parameters: the Fe(1)–C(13)–C(14) angle, ϕ, the Fe(2)–C(13)–C(14) angle, χ, and rotation, θ, of the ester function about the C(13)–C(14) bond (Figure 1). As discussed above, contributions from the iron and the dummy atoms were not included.

Coordinates for all non-hydrogen atoms of the acetyl derivative $[Fe_4(CO)_{12}C\cdot C(O)CH_3]^-$, II, were likewise taken from the single-crystal X-ray analysis (Table III). Although approximate hydrogen atoms positions were also determined, they are of limited precision and they were therefore replaced by hydrogen atoms added geometrically as above. Dummy atoms V1 and V2 were added and the calculations pursued as for the carbomethoxy derivative.

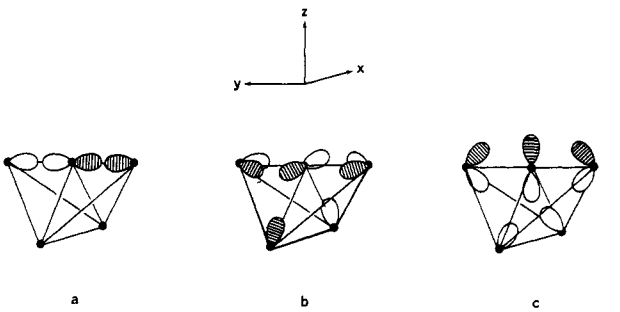

Figure 4. Schematic representations of the bonding interactions between the carbido carbon p_y (a), p_x (b), and p_z (c) orbitals and the iron framework orbitals in $[Fe_4C(CO)_{12}]^{2-}$ (ref 7). The local coordinate system on the carbon atoms is defined as shown.

Results and Discussion

1. Molecular and Electronic Structure. The structures of both I and II are similar in many respects. The Fe_4 cores in both clusters take on the now familiar open butterfly configuration, each vertex bearing three essentially linear terminal carbonyl ligands (Figures 1 and 2). The dihedral angle between the two triangular wings of the cluster is 130° for I and 128° for II. The Fe–Fe distances in each cluster fall into two groups. The Fe(1,4)–Fe(2,3) distances (between the wingtip and backbone iron atoms) are 2.50 ± 0.01 Å in I and 2.51 ± 0.01 Å in II; the Fe(1)–Fe(4) distances are significantly greater, 2.59 Å in I and 2.57 Å in II.

In both cluster anions the methylidyne carbon is situated outside the Fe_4 polyhedron ca. 0.5 Å from the Fe(2)–Fe(3) vector (compared with 0.06 Å for the parent $Fe_4C(CO)_{13}$ molecule[29]) resulting in Fe(2)–C(13)–Fe(3) angles of 148° and 149° for I and II, respectively. The wingtip iron to methylidyne carbon distances (Fe(2),(3)–C(13)) are similarly longer (2.017 ± 0.007 Å in I, 2.009 ± 0.002 Å in II) than the backbone iron to methylidyne carbon distances (1.950 ± 0.009 Å in I, 1.967 ± 0.003 Å in II). The two anions differ structurally in one important respect. In I the carbomethoxy group lies approximately in both the Fe(1)C(13)Fe(4) plane and the Fe(2)C(13)Fe(3) plane, with Fe(2)–C(13)–C(14) = 105.1°, Fe(3)–C(13)–C(14) = 106.9°, Fe(1)–C(13)–C(14) = 137.6°, and Fe(4)–C(13)–C(14) = 139.2°. In II the acetyl group lies approximately in the Fe(1)C(13)Fe(4) plane (Fe(3)–C(13)–C(14) = 106.6°, Fe(2)–C(13)–C(14) = 104.7°) but is tilted out of the Fe(2)C(13)Fe(3) plane by about 5° toward Fe(1) (Fe(1)–C(13)–C(14) = 134.4°, Fe(4)–C(13)–C(14) = 143.9°). The angles about the organic carbonyl carbon atoms C(14) in I and II approximate the trigonal geometry appropriate for a formally sp^2 carbon atom, with I showing the greater deviation in a closing of the C(13)–C(14)–O(14) angle to 111°.

It is instructive to compare the geometry of the Fe_4C cores in I and II with those found in the Fe_4C clusters that bear no substituent on the carbide carbon atom. The three related clusters in this group, $Fe_4C(CO)_{13}$, $[HFe_4C(CO)_{12}]^-$, and $[Fe_4C(CO)_{12}]^{2-}$, have all been characterized previously

(18) White, D. N. J., *Spec. Period. Rep. (Chem. Soc.)* **1978**, *No. 6*, 38.
(19) Hopfinger, A. J. *Conformational Properties of Macromolecules*; Academic Press: New York, 1979.
(20) Burkert, U.; Allinger, N. L. *Molecular Mechanics*; American Chemical Society: Washington, DC, 1982.
(21) Brubaker, G. R.; Johnson, D. W. *Coord. Chem. Rev.* **1984**, *53*, 1–36.
(22) Brubaker, G. R.; Johnson, D. W. *Inorg. Chem.* **1984**, *23* 1591–1595.
(23) Adam, K. R.; Brigden, L. G.; Henrick, K.; Lindoy, L. F.; McPartlin, M.; Mimnagh, B.; Tasker, P. A. *J. Chem. Soc., Chem. Commun.* **1985**, 710–711.
(24) Boeyens, J. C. A.; Cotton, F. A.; Han, S. *Inorg. Chem.* **1985**, *24*, 1750–1753.
(25) Bond, A. M.; Hambley, T. W.; Snow, M. R. *Inorg. Chem.* **1985**, *24*, 1920–1928.
(26) Boeyens, J. C. A. *Inorg. Chem.* **1985**, *24*, 4149–4152.
(27) Lauher, J. W. *J. Am. Chem. Soc.* **1986**, *108*, 1521–1531.
(28) Davies, E. K. *CHEMGRAF Program Suite*; Chemical Crystallography Laboratory, University of Oxford: Oxford, England, 1982.

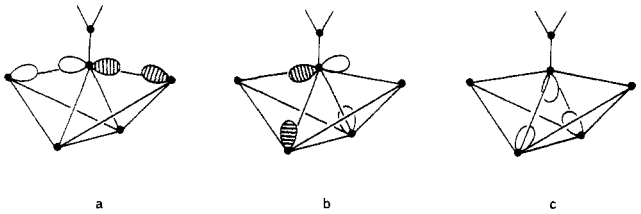

Figure 5. Schematic representations of the bonding interactions between the μ_4-methylidyne carbon p_y (a), p_x (b), and p_z (c) orbitals and the iron framework orbitals in $[Fe_4(CO)_{12}C{\cdot}C(O)OCH_3]^-$. The coordinate system on the carbon atom is defined as in Figure 4.

by X-ray diffraction,[29,11,8] and they share a remarkably invariant core geometry. The butterfly dihedral angle is 102 ± 2°, the angle at the carbide carbon subtended by the wingtip iron atoms is 176 ± 2°, and the two sets of iron–carbide distances are 1.79 ± 0.01 Å from the wingtip iron atoms and 1.97 ± 0.03 Å from the backbone iron atoms. The consistency of this geometry with the bonding in these clusters has been established by Fenske–Hall[7] and extended Hückel[6] molecular orbital calculations. These studies show that the observed location of the carbide carbon atom in the three Fe_4C clusters maximizes the σ interaction between the carbon $2p_y$ orbital and the wingtip iron atoms as well as the σ and π interactions between the carbon $2p_x$ and $2p_z$ orbitals and the backbone and wingtip iron atoms (Figure 4). In forming derivatives such as I and II this bonding scheme is disrupted. Because the iron butterfly has opened up, giving a wider dihedral angle (129 ± 1°) and longer iron–carbon bond distances for the wingtip iron atoms, the methylidyne carbon is now ca. 0.5 Å above a vector connecting the two wingtip iron atoms. This change in geometry, combined with the fact that the methylidyne carbon is now bound to another carbon atom as well as to the iron framework, is reflected in the bonding betwen the methylidyne carbon and the iron framework. The carbon p_z orbital, hybridized with the 2s orbital, is used in bonding to the adjacent carbon, so that the interaction of the p_z orbital with the iron framework is replaced by the interaction of a sp lone pair type orbital on the methylidyne fragment with the iron atoms. A σ interaction between this methylidyne orbital and the backbone iron atoms remains in I and II, but a π-type interaction between the carbon p_z orbital and the wingtip iron atoms cannot occur (Figure 5c). The carbon p_x orbital is not used for bonding within the methylidyne group and is thus available for bonding to the iron framework. The folding back of the wingtip iron atoms, however, results in almost complete loss of π bonding between the carbon p_x orbital and the wingtip iron atoms. This loss is mitigated by strengthened interactions between the p_x orbital and the backbone iron atoms (Figure 5b). Finally, the interaction of the carbon p_y orbital with the iron framework is affected by both the folding back of the wingtip iron atoms and bonding with the adjacent carbon atom. The bending back of the wingtip iron atoms weakens the bond between the methylidyne carbon p_y orbital and the wingtip iron atoms (Figure 5a), but the carbon p_y orbital is stabilized by bonding with the adjacent carbon atom. The planar configuration of the methylidyne group and the sp^2 hybridization of the adjacent carbonyl carbon allow the development of some π bond character between the carbide carbon and the sp^2 carbon. To summarize, in methylidyne derivatives such as I and II the carbide carbon p_z and p_y orbitals are used in bonding with the iron framework and within the methylidyne group. The carbon p_x orbital is used only for bonding to the iron framework. These changes in bonding that occur upon derivatization of the carbide carbon atom can be seen by comparing the schematic diagrams of the carbon–iron interactions in $[Fe_4C(CO)_{12}]^{2-}$ and $[Fe_4(CO)_{12}C{\cdot}C(O)OCH_3]^-$ (I) (Figures 4 and 5). They are also reflected in the different values of the carbon–iron overlap populations in $[Fe_4C(CO)_{12}]^{2-}$, I, and II (Table VI).

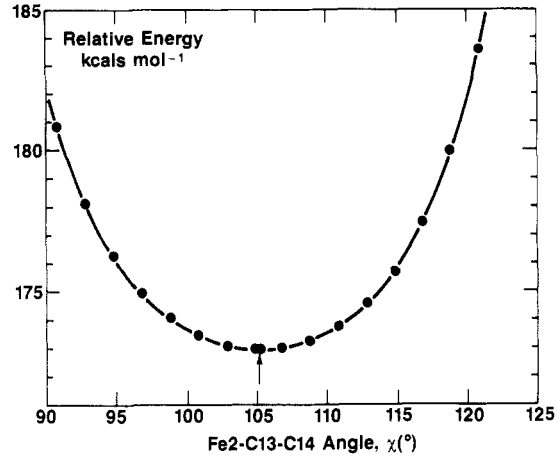

Figure 6. A plot of the relative nonbonded intramolecular interaction energy for the carbomethoxy derivative, $[Fe_4(CO)_{12}C{\cdot}C(O)OCH_3]^-$, I, plotted as a function of the Fe(2)–C(13)–C(14) angle, χ. Mulliken atomic charges derived in the Fenske–Hall MO analysis[7] were used in evaluating coulombic contributions. In the crystal structure χ is found to be 105.1° (indicated by the arrow).

2. Steric Constraints. The molecular orbital calculations show that the orientation of the organic group in the carbomethoxy derivative I allows effective bonding between the methylidyne carbon and all directly bonded atoms. It has been suggested alternatively[6] that this orientation is determined by steric, i.e. nonbonded, interactions between the organic group and the nearest carbonyl ligands in this cluster. The interactive molecular modeling was used to evaluate this possibility. Figure 6 shows the total nonbonded energy sum as a function of the Fe(2)–C(13)–C(14) angle, χ, computed with the inclusion of Coulombic terms based on the Mulliken atomic charges derived from the Fenske–Hall MO analysis. The energy minimum calculated either with or without inclusion of the Coulombic terms coincides within one degree with the configuration observed crystallographically. The minimum is relatively sharp and even small changes in the Fe(2)–C(13)–C(14) angle, χ, are accompanied by significant increases in the nonbonded energy sum. Even allowing considerable margin for the approximate nature of the present methodology (see above), the carbomethoxy group is indeed seen to be constrained sterically to a configuration close to that observed crystallographically.

There are similar steric constraints on other rotations of the carbomethoxy group. Figures 7–9 are contour plots of the energy surface of the ester group as a function of the Fe(2)–C(13)–C(14) angle, χ, and the V1–C(13)–C(14)–O(14) torsion angle, θ (Figure 7), the Fe(1)–C(13)–C(14) angle, ϕ, and θ (Figure 8), and χ and ϕ (Figure 9). The contour spacing corresponds in each case to a change in computed energy of 1 kcal mol^{-1} (kT = 0.59 kcal mol^{-1}). The crystallographic configuration (χ = 105.1°, ϕ = 137.6°, θ = −0.5°) in each case lies within the lowest computed energy contour. The steric constraints on the orientation of the carbomethoxy group in I thus complement the orbital overlap effects described above.[7]

(29) Bradley, J. S.; Ansell, G. B.; Leonowicz, M. E.; Hill, E. W. *J. Am. Chem. Soc.* **1981**, *103*, 4968–4970.

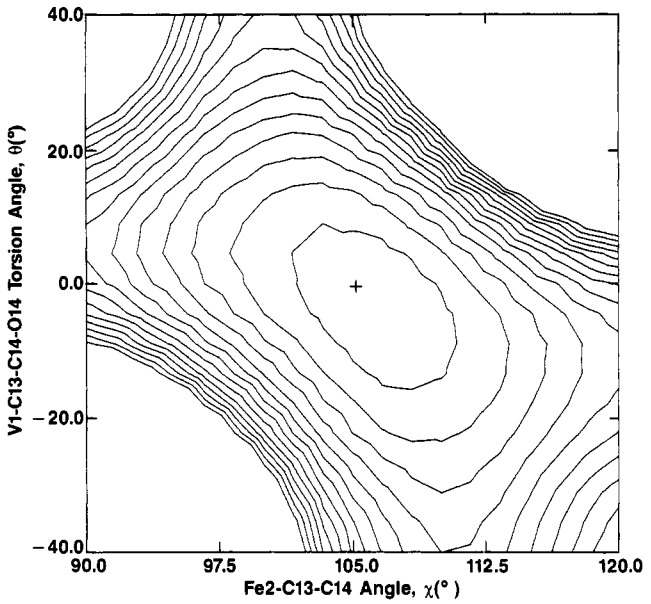

Figure 7. A contour plot of the relative intramolecular nonbonded interaction energy for I plotted as a function of the Fe(2)–C(13)–C(14) angle, χ (horizontal axis), and the V1–C(13)–C(14)–O(14) torsion angle, θ (vertical). The computed contour level spacing is 1 kcal mol^{-1}. The conformation observed in the crystal structure lies within the lowest computed energy contour (indicated by the +).

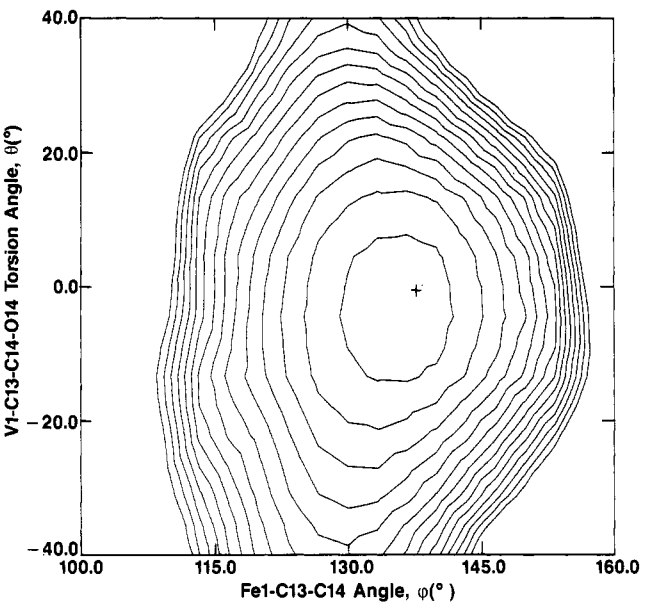

Figure 8. A contour plot of the relative intramolecular nonbonded interaction energy for I plotted as a function of the Fe(1)–C(13)–C(14) angle, ϕ (horizontal), and θ (vertical). Further details are as for Figure 7.

In contrast to the orientation of the carbomethoxy group in I, the orientation of the acetyl group in II is not axial with respect to the iron butterfly but is rather tilted to the side opposite the methyl group, such that the Fe(4)–C(13)–C(14) angle is some 10° larger than the Fe(1)–C(13)–C(14) angle. In the Fe(2)C(13)Fe(3) plane, by comparison, the Fe(2)–C(13)–C(14) and Fe(3)–C(13)–C(14) angles are almost equal. This difference between the acetyl and carbomethoxy derivatives can be readily understood in terms of the differing steric requirements of the two organic groups. Figure 10 shows the nonbonded intramolecular interaction energy plotted as a function of the Fe(1)–C(13)–C(14) angle, ϕ. The orientation of the acetyl group observed crystallographically occurs at a computed

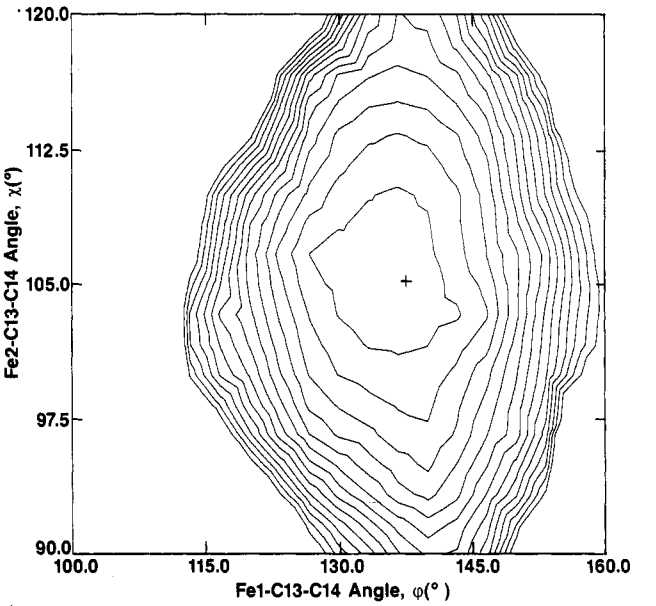

Figure 9. A contour plot of the relative intramolecular nonbonded interaction energy for I plotted as a function of ϕ (horizontal) and χ (vertical). Further details are as for Figure 7.

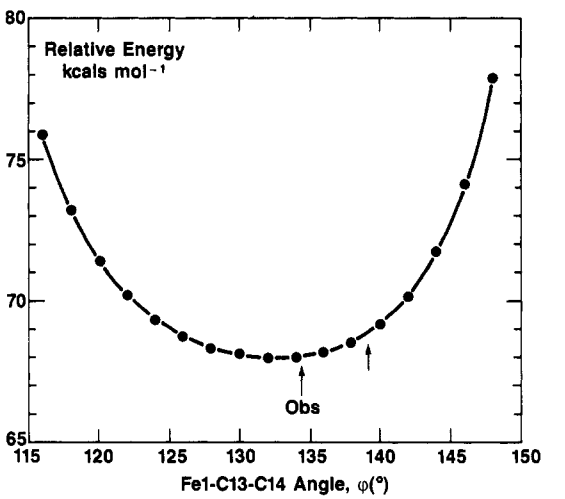

Figure 10. A plot of the relative intramolecular nonbonded interaction energy of the acetyl derivative, $[Fe_4(CO)_{12}C{\cdot}C(O)CH_3]^-$, II, plotted as a function of the Fe(1)–C(13)–C(14) angle, ϕ. No coulombic terms were included. In the crystal structure ϕ is found to be 134.4° (indicated by the arrow labeled "obs"). A value of ϕ = 139.2° (indicated by the second arrow) would correspond to equal values of the Fe(1)–C(13)–C(14) and Fe(4)–C(13)–C(14) angles.

energy very close to the minimum and significantly lower than that for a value ϕ = 139.2°, which would correspond to an axial orientation of the group (equal Fe(1)–C(13)–C(14) and Fe(4)–C(13)–C(14) angles).

The availability of structural data for more than one iron butterfly cluster derivative enables us also to consider the possible predictive power of these simple interactive molecular graphics techniques. Specifically, the predicted orientation of the acetyl group in a hypothetical model cluster derived from the carbomethoxy derivative was compared with that observed crystallographically. Taking the molecular structure of the carbomethoxy derivative as the basis for the hypothetical cluster, C(15) and the methyl hydrogen atoms H(34), H(35), and H(36) were deleted. O(14) was converted to C(21) and its position adjusted to give a C(14)–C(21) bond length of 1.50 Å (the value observed in the crystal structure of the acetyl derivative is 1.503 Å). The C(13)–C(14)–C(21) bond angle was then

Table VII. Comparison of the Observed and "Calculated" Orientations of the Acetyl Group in $[Fe_4(CO)_{12}C \bullet C(O)CH_3]$

angle	obsd, deg	calcd, deg
Fe(1)-C(13)-C(14) (ϕ)[a]	134.4	129.0
Fe(4)-C(13)-C(14)	143.9	147.9
Fe(2)-C(13)-C(14) (χ)[a]	104.7	105.4
Fe(3)-C(13)-C(14)	106.6	106.0
Fe(1)-C(13)-C(14)-O(13) (θ)[a]	-1.5	-5.2

[a] See text.

adjusted to a value of 120°, expected for regular sp^2 hybridization at C(14) (the observed value is 119.2°). Three hydrogen atoms were added to C(21) as above. The orientation of the group was then optimized by an iterative series of automatic adjustments of the torsion angles about C(21)-C(14), C(14)-C(13), and C(13)-V1 or, separately, C(13)-V2. This "predicted" geometry is compared with that observed in the crystal structure in Table VII. The calculated angles in the optimized orientation (based on the skeleton of I) are within a few degrees of those actually observed in II. The simple modeling of this hypothetical cluster clearly predicts the observed tilt of the acetyl group toward Fe(1) in the Fe(1)Fe(3)C(13)C(14) (approximate) plane. It is important to emphasize that this prediction does not derive from a comparison of the total nonbonded interaction energy sums for the two derivatives. The methods used here provide only a means of mapping the nonbonded energy terms as a function of changes in the conformation of each molecule and, hence, a means of deriving conformations that are optimized only with respect to this description of the nonbonded atom-atom interactions within that molecule. The absolute values of the nonbonded energy sums cannot easily be compared because, as discussed above, the nonbonded terms are only one component of the total cluster Hamiltonian.

It has been suggested by Shriver and co-workers[30,31] that the use of a Buckingham potential to evaluate C-C repulsions in carbonyl clusters overestimates the "hardness" of the carbon atoms, giving rise to unrealistically high interatomic repulsive energy terms. It is therefore valid to question whether the peaks and troughs in the computed nonbonded interaction energy surface for the organic group in the environment provided by the carbonyls are overemphasized. Whether, that is, a small (and presumably energetically insignificant) perturbation of the carbonyl configuration might be sufficient to permit the acetyl group in II to adopt the axial orientation found for the carbomethoxy group in I. This question is resolved quantitatively for the present system by the crystallographic results. The distributions of carbonyl ligands about the cluster cores in these types of systems are dictated mainly by ligand-ligand nonbonded interactions[27] (Figure 3). These interactions are such that the relative dispositions of the carbonyl groups in the carbomethoxy (I) and acetyl derivatives (II) are similar, enabling a sensible indication of the molecular structure of II to be generated on the basis of the geometry of the $Fe_4(CO)_{12}C$ core in I. That is not to say that the carbonyl configuration is completely static. Accommodation of the acetyl group in II results in subtle readjustments of the cluster components. The Fe(1)-Fe(4) distance in II is 0.015 Å shorter than that in I (Table IV) and, correspondingly, the Fe(1)-V3-Fe(4) angle (V3 is the midpoint of the Fe(2)-Fe(3) vector) in II (107.4°) is more acute than in I (110.2°). The carbonyl groups on Fe(1) (labeled 1,2, and 3) and on Fe(4) (labeled 10, 11, and 12) are rotated by about 2° in II relative to I, as is illustrated by the torsion angles in Table V. The angle about Fe(4) to the carbonyl ligand directly beneath the methyl function of the acetyl group (C(12), O(12)) is also slightly more obtuse in the acetyl derivative (Fe(1)-Fe(4)-C(12) = 154.7°, Fe(4) - Fe(1)-C(2) = 151.4°) than in the carbomethoxy derivative (Fe(1)-Fe(4)-C(12) = 150.9° and Fe(4)-Fe(1)-C(2) = 152.6°). Each of these subtle effects, which were not included in constructing the hypothetical model of the acetyl derivative, could facilitate accommodation of the acetyl group. As a result of the latter effect, in particular, the "calculated" tilt of the acetyl group away from the methyl group side is slightly *larger* than that actually observed (Table VII). Although proper incorporation of each of these relaxation effects is beyond the capabilities of the present methodology, their inclusion may be essential for similar comparisons in other organometallic systems in which overall molecular relaxations are less limited.

3. Bonding vs. Nonbonded Interactions. Although we have not attempted to compute total energies for these clusters by molecular orbital calculations (a prohibitive task), we are able to comment on the effect of tilting the acetyl group on the bonding in II. The question is simply whether or not the sterically induced displacement of the acetyl group in II (away from the axial orientation which optimizes bonding interactions in I) is noticeably resisted by the bonding requirements of the cluster. The results of molecular orbital calculations for II suggest that it is not.

The diagrams in Figure 5 represent the carbon-metal interactions when the organic group has an axial orientation, as in I. How are these interactions affected by movement of the acetyl group? First, the tilt of the acetyl group in the Fe(1)C(13)Fe(4) plane has no effect on the interactions between the carbon p_y orbital and the iron framework shown in Figure 5a for an axial ligand. The individual metal-carbon interactions involving the carbon p_z and p_x orbitals are affected by the tilt of the acetyl group, however, because a change in orientation of that group changes the orientation of the carbon p_z and p_x orbitals with respect to the iron atoms in the backbone of the butterfly. When the acetyl group is tipped over toward Fe(1), the carbon sp type hybrid orbital shown in Figure 5c is tipped toward Fe(4), and the p_x orbital, shown in Figure 5b as parallel to the Fe(1)-Fe(4) bond, tips over so that one lobe is closer to Fe(1). Thus, the carbon p_z interacts more strongly with Fe(4) than with Fe(1), while the p_x orbital interacts more strongly with Fe(1). These differences can be seen by comparing the metal-carbon overlap populations listed in Table VI for the two backbone iron atoms in II. It is particularly interesting to note when comparing these values that the changes in the interactions involving the p_z and p_x orbitals compensate one another so that overall the strength of the carbon-metal interactions involving the backbone iron atoms is little changed from that observed in I. Thus, it appears that since the movement of the acetyl group is confined to the Fe(1)C(13)Fe(4) plane steric repulsions can be minimized without disrupting bonding. Movements out of this plane, however, would have a much more substantial effect on these bonding interactions.

Conclusion

The crystal, molecular, and electronic structures of two derivatized iron butterfly clusters, $[Fe_4(CO)_{12}C \cdot C(O)OCH_3]^-$, I, and $[Fe_4(CO)_{12}C \cdot C(O)CH_3]^-$, II, have been described. The structures are similar, and the corresponding

(30) Horwitz, C. P.; Holt, E. M.; Shriver, D. F. *Inorg. Chem.* **1984**, *23*, 2491-2499.
(31) Bogdan, P.; Horwitz, C. P.; Shriver, D. F. *J. Chem. Soc., Chem. Commun.* **1986**, 553-555.

Fe–Fe distances and the dihedral angles between the two triangular wings of the cluster are nearly identical in I and II. Compared to Fe_4C clusters containing an underivatized carbido carbon, the wingtips of the cluster in I and II are opened up to give a greater dihedral angle and longer Fe–C distances for the wingtip Fe atoms. In both I and II, the carbon p orbitals, which in the underivatized Fe_4C clusters were used only for bonding with the cluster Fe atoms, are now used for bonding within the organic group as well as for cluster bonding. Steric constraints on the orientations of the carbomethoxy group in I and on the acetyl group in II were examined in a semiquantitative fashion by using simple interactive molecular graphics routines. In I, the observed axial orientation of the organic group that optimizes bonding interactions is found also to minimize steric repulsions. In II the observed off-axis tilt of the acetyl group is shown similarly to reflect steric constraints. The molecular orbital calculations suggest that bonding interactions are not disrupted by this reorientation of the organic group in the Fe(1)Fe(4)C(14) (approximate) plane. The interactive molecular graphics routines were also used to generate a model for the structure of II based on the molecular structure of the $Fe_4(CO)_{12}C$ core in I. The reasonable correspondence between the observed and "predicted" orientations of the acetyl group demonstrates the possible utility of these simple methods in predicting certain cluster conformations.

Acknowledgment. The authors acknowledge with gratitude a stimulating correspondence with Professor D. F. Shriver on the subject of molecular graphics and its limitations and for access to a preprint of ref 31.

Registry No. I, 72872-04-9; II, 99922-06-2; $Et_4N[HFe_4C(CO)_{12}]$, 79723-27-6; $(Et_4N)_2[Fe_4C(CO)_{12}]$, 83270-11-5; $(Et_4N)_2[Fe_6C(CO)_{16}]$, 11087-55-1; $FeCl_3$, 7705-08-0.

Supplementary Material Available: Tables of anisotropic thermal parameters for I and II (4 pages); tables of structure factors for I and II (30 pages). Ordering information is given on any current masthead page.

Preparation and Reactions of an Alkylzinc Enolate

Marvin M. Hansen, Paul A. Bartlett, and Clayton H. Heathcock*

Department of Chemistry, University of California, Berkeley, California 94720

Received December 23, 1986

The preparation, characterization, and reactivity of ethylzinc enolate **3** are reported. Enolate **3** is less reactive than the corresponding lithium enolate but undergoes many of the same reactions. The unprecedented protonation of **3** by secondary amines is reported. The metal exchange reaction used to prepare **3** is not a general method for the preparation of other alkylzinc enolates.

Recent interest in the stereochemistry of the aldol addition reaction[1] has resulted in significant interest in the specific generation and characterization of metal enolates.[2,3] Those involving zinc have received less attention, although they would appear to offer additional coordination sites for the incorporation of auxiliary ligands for stereocontrol. The most general methods for the direct generation of zinc enolates are metal exchange between lithium enolates and zinc chloride[4] and reduction of α-bromo carbonyl compounds, as in the Reformatsky reaction.[5] In addition to these methods for preparing halozinc enolates, there are a few reports on the synthesis of alkylzinc enolates. Dialkylzinc reagents are useful polymerization catalysts; however, addition of diethylzinc to chalcone affords a stable ethylzinc enolate which has been characterized (eq 1).[6] The direct synthesis of *n*-butyl(dimethyl malonato)zinc by deprotonation of dimethyl malonate with di-*n*-butylzinc has been demonstrated (eq 2).[7] This approach is probably not applicable to the synthesis of nonactivated ketone enolates due to the low basicity of dialkylzinc reagents.[8] Boersma and co-workers[4b] have reported that the exchange reaction between ethylzinc methoxide and enol acetates affords ethylzinc enolates that decompose by polymerization or by reaction

(1) For reviews of the aldol reaction, see: (a) Mukaiyama, T. *Organic Reactions*; Wiley: New York, 1982; Vol. 28, p 203. (b) Heathcock, C. H. In *Asymmetric Synthesis*; Morrison, J. D., Ed.; Academic: New York, 1984; Vol. 3, p 111. (c) Evans, D. A.; Nelson, J. V.; Taber, T. R. *Top. Stereochem.* **1982**, *13*, 1.

(2) For crystallographic structural studies of group I (11) and II (12) metal enolates, see: (a) Williard, P. G.; Carpenter, G. B. *J. Am. Chem. Soc.* **1986**, *108*, 462; **1985**, *107*, 3345. (b) Amstutz, R.; Dunitz, J. D.; Laube, T.; Schweizer, W. B.; Seebach, D. *Chem. Ber.* **1986**, *119*, 434. (c) Williard, P. G.; Salvino, J. M. *J. Chem. Soc., Chem. Commun.* **1986**, 153. (d) Seebach, D.; Amstutz, R.; Laube, T.; Schweizer, W. B.; Dunitz, J. D. *J. Am. Chem. Soc.* **1985**, *107*, 5403. (e) Laube, T.; Dunitz, D. J.; Seebach, D. *Helv. Chim. Acta* **1985**, *68*, 1373. (f) Bauer, W.; Laube, T.; Seebach, D. *Chem. Ber.* **1985**, *118*, 764. (g) Jastrzebski, J. T. B. H.; van Koten, G.; Christophersen, M. J. N.; Stam, C. H. *J. Organomet. Chem.* **1985**, *292*, 319. (h) Amstutz, R.; Schweizer, W. B.; Seebach, D.; Dunitz, J. D. *Helv. Chim. Acta* **1981**, *64*, 2617. (i) Cambillau, C.; Bram, G.; Corset, J.; Riche, C. *Can. J. Chem.* **1982**, *60*, 2554; *Nouv. J. Chim.* **1979**, *3*, 9. (j) Riche, C.; Pascard-Billy, C.; Cambillau, C.; Bram, G. *J. Chem. Soc., Chem. Commun.* **1977**, 183. (k) Jackman, L. M.; Lange, B. C. *Tetrahedron* **1977**, *33*, 2737 and references therein.

(3) For crystallographic structural studies of transition-metal enolates, see: (a) Heathcock, C. H.; Doney, J. J.; Bergman, R. G. *Pure Appl. Chem.* **1985**, *57*, 1789 and ref 26 and 27 therein. (b) Doney, J. J.; Bergman, R. G.; Heathcock, C. H. *J. Am. Chem. Soc.* **1985**, *107*, 3724. (c) Grassi, A.; Longo, P.; Musco, A.; Porzio, W.; Scrivanti, A. *J. Organomet. Chem.* **1985**, *289*, 439. (d) Planalp, R. P.; Andersen, R. A. *J. Am. Chem. Soc.* **1983**, *105*, 7774. (e) Moore, E. J.; Straus, D. A.; Armantrout, J.; Santarsiero, B. D.; Grubbs, R. H.; Bercaw, J. E. *Ibid.* **1983**, *105*, 2068. (f) Czauderna, B.; Jogun, K. H.; Stezowski, J. J.; Foehlisch, B. *Ibid.* **1976**, *89*, 6696. (g) Mercury enolate: Potenza, J. A.; Zyontz, L.; San Filippo, J.; Lancette, R. A. *Acta. Crystallogr., Sect. B: Struct. Crystallogr. Cryst. Chem.* **1978**, *B34*, 2624.

(4) See the seminal paper by House: (a) House, H. O.; Crumine, D. S.; Teranishi, A. Y.; Olmstead, H. D. *J. Am. Soc. Chem.* **1973**, *95*, 3310. See the recent work by Boersma where self-condensation of chlorozinc enolates was observed: (b) Dekker, J.; Schouten, A.; Budzelaar, P. H. M.; Boersma, J.; van der Kerk, G. J. M. *J. Organomet. Chem.* **1987**, *320*, 1.

(5) (a) Shiner, R. L. *Org. React. (N.Y.)* **1942**, *1*, 1. (b) Frankenfeld, J. W.; Werner, J. J. *J. Org. Chem.* **1969**, *34*, 3689. (c) Rathke, M. W.; Lindert, A. *Ibid.* **1970**, *35*, 3966. (d) Dekker, J.; Budzelaar, P. H. M.; Boersma, J.; van der Kerk, G. J. M.; Speck, A. L. *Organometallics* **1984**, *3*, 1403.

(6) (a) Tsushima, R.; Tsuruta, T. *Makromol. Chem.* **1973**, *166*, 325. (b) Boersma, J.; Noltes, J. G. *Recl. Trav. Chim. Pays-Bas* **1973**, *92*, 229.

(7) Kawakami, Y.; Tsuruta, T. *Bull. Chem. Soc. Jpn.* **1971**, *44*, 247.

(8) Inoue, S.; Imanaka, Y. *J. Organomet. Chem.* **1972**, *35*, 1.

0276-7333/87/2306-2069$01.50/0